

Photonic bandgap fiber tapers and in-fiber interferometric sensors

Jian Ju,¹ Lina Ma,^{1,2} Wei Jin,^{1,*} and Yongming Hu²

¹Department of Electrical Engineering, Hong Kong Polytechnic University, Hung Hom, Kowloon, Hong Kong

²College of Optoelectronic Science and Technology, National University of Defense Technology, Changsha, Hunan 410073, China

*Corresponding author: eewjin@polyu.edu.hk

Received April 8, 2009; revised May 12, 2009; accepted May 12, 2009;
posted May 20, 2009 (Doc. ID 109671); published June 11, 2009

Nonadiabatic tapers in hollow-core air-silica photonic bandgap fibers (PBFs) were fabricated by the use of a fiber fusion splicer. In addition to the well-known scaling down of fiber dimensions, the innermost rings of air holes were found collapsed or significantly deformed, which results in almost doubling the diameter of the hollow core in the tapered region. The tapering of the PBF causes coupling of the fundamental core mode to a surface mode with $\sim 10\%$ higher effective mode index. An in-fiber core-surface mode interferometer was constructed by cascading two such tapers along the PBF. The interferometer was experimentally demonstrated for strain and temperature measurement, and the sensitivities of the interferometric peak wavelength to strain and temperature are measured to be $-0.64 \text{ pm}/\mu\epsilon$ and $495.6 \text{ pm}/(^{\circ}\text{C m})$, respectively.

© 2009 Optical Society of America

OCIS codes: 060.2310, 060.2370, 060.2340.

Photonic bandgap (PBG) fibers (PBFs) rely on the PBG effect exhibited by the photonic crystal cladding (PCC) to guide light and allow the confinement of light in an air core [1,2]. The very low overlap between the light field and the glass facilitates light transmission with lower nonlinearity, higher damage threshold, and potentially extremely low-loss transmission beyond the Rayleigh limit [3]. By filling the hollow-core/cladding holes with gas or liquid, PBFs provide excellent platforms for studying light/matter interaction over long lengths [4,5]. We have recently fabricated long-period gratings (LPGs) in air-core PBFs and demonstrated that such LPGs have very small sensitivity to temperature, bend, and external refractive index, but large sensitivity to strain [6]. In this Letter, we report the fabrication of nonadiabatic tapers in air-core PBFs and study the mode coupling occurring at such tapers.

Conventional fiber tapers have been extensively investigated as fused couplers, narrowband filters, for mode matching between waveguides, and for mode coupling [7,8]. From a geometrical point of view, adiabatic tapers have a small taper angle along the length of the device and thereby minimize the coupling to higher-order cladding modes. Conversely, nonadiabatic tapers allow power exchange between fundamental and higher order modes, resulting in interferometric devices [9,10]. Recently, fabrication and characterization of tapered air-core PBFs have been reported [11]. Preliminary results showed that even weak tapers with small reduction in the fiber outer diameter can cause coupling to cladding modes, although the details of the cladding modes were not reported. The refractive index difference between the coupled modes was found to be much higher than that in conventional single-mode fibers (SMFs).

In this Letter we show that a strong or nonadiabatic taper not only scales down the fiber dimension but also enlarges the central air-core size. This induces coupling of fundamental mode to a surface

mode with its mode field mainly distributed around the core-cladding boundary. We will also demonstrate an in-fiber core-surface mode interferometer by cascading two such tapers and apply it for strain and temperature measurement.

The PBF used is Crystal Fiber A/S's HC-1550-02 with cross section shown in Fig. 1(a). The PBF has an air core with a diameter of $12.5 \mu\text{m}$, surrounded by a PCC comprising a triangular array of air holes in a silica background. The average spacing between the air holes is $4.7 \mu\text{m}$. A taper program was developed on a conventional fusion splicer (Ericsson FSU 975) so that it can automatically fabricate tapers with good repeatability. Before tapering, short pieces ($\sim 5 \text{ cm}$) of PBFs were spliced to conventional SMFs at both ends, and the total splice loss is $\sim 6.5 \text{ dB}$. After removing the polymer coating, the PBFs were then tapered and the transmission spectra were recorded for further analysis. The tapers are characterized by tapering ratio, which is defined as $\Delta R/R$, where ΔR is the reduction in the fiber radius at the taper waist and $R=63 \mu\text{m}$ is the outer radius of the original PBF. The cross section of the tapered PBF waist is shown in Fig. 1(b), and the side image of a particular tapered region is shown in Fig. 1(c). The outer diameter has been reduced from 126 to $98 \mu\text{m}$

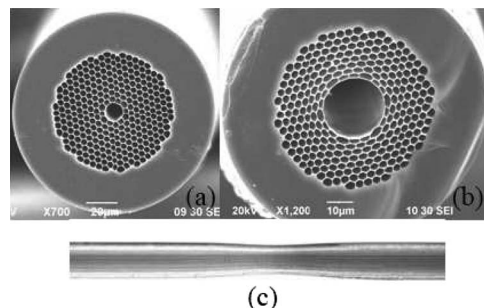


Fig. 1. Scanning electron microscopy images of (a) untapered and (b) tapered PBF cross sections. (c) Side view of the tapered region.

($\Delta R/R=22\%$). The innermost ring of the air hole was found completely collapsed, and the central core of the PBF was found enlarged to $24\ \mu\text{m}$. The two rings of air holes adjacent to the central core were partially deformed from their original hexagon shape, while other air holes retained their shapes but were scaled down proportionally.

Figure 2 shows the transmitted spectra of the PBF before and after a single taper was fabricated. The spectra are normalized to the source spectrum measured from its SMF pigtail. Several observations may be made from Fig. 2. First, the transmission loss of the PBF with taper increases significantly but gradually with a wavelength of beyond $1530\ \text{nm}$. This is believed to be due to the shift of the PBG of the tapered PBF. Considering only the scaling down ($\Delta R/R=22\%$) of the fiber cross section in the tapered region while the air filling ratio is kept as 94% , the transmission window was theoretically estimated to shift from 1.38 – $1.42\ \mu\text{m}$ for the original PBF to 1.08 – $1.42\ \mu\text{m}$ for a PBF of the dimension of the taper waist. However, since the 22% reduction in dimension occurred gradually in the short tapered region of 150 – $250\ \mu\text{m}$ in length, the transmission loss is then expected to increase gradually with the wavelength, rather than sharply as manifested by a long length of the uniform PBF. Second, the short-wavelength edge of the transmitted spectrum for the PBF with a taper shows no obvious difference from the PBF without the taper. This is expected because this edge is limited by the relatively long sections of the unmodified PBF on input/output sides of the tapered region. Third, the periodic ripples in the transmitted spectrum of the tapered PBF increased in amplitude as compared with that of the untapered PBF. We believe, as will be discussed later, that it is owing to the excitation of surface modes that interfere with the fundamental mode and produce interference fringes.

To understand the mode coupling characteristics, we made an in-fiber Mach–Zehnder interferometer (MZI) by fabricating two tapers separated by $23\ \text{mm}$ along the same PBF as shown in Fig. 3(a). The transmitted spectrum of the device is shown in Fig. 3(b). The spectrum is quasi-sinusoidally modulated over a wavelength range larger than $50\ \text{nm}$, indicating that

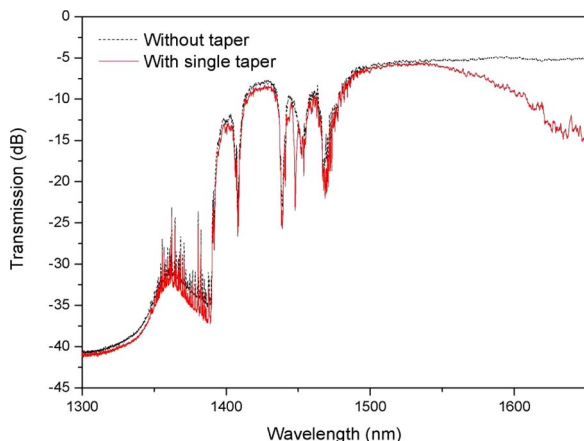


Fig. 2. (Color online) Transmission spectra of a PBF with and without a taper.

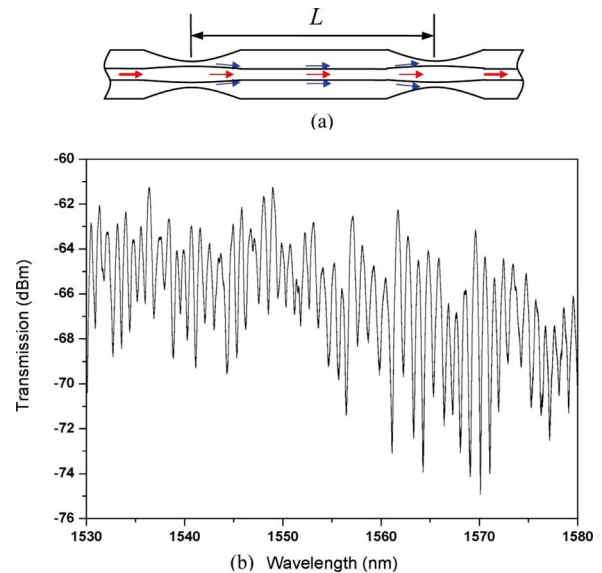


Fig. 3. (Color online) (a) In-fiber MZI and (b) its transmission spectrum.

the mode conversion occurs over a much broader band than the resonant mode coupling as observed in LPGs in PBFs, which are $\sim 5.6\ \text{nm}$ [6]. The approximately even spacing between the interference peaks indicates that the detuning between coupled modes is weak and that possibly a single mode is dominantly coupled from the fundamental mode.

Plenty of information may be obtained from the interference fringes. For an MZI, the wavelength spacing ($\Delta\lambda$) between two adjacent transmission peaks and the effective index difference (Δn) between the coupled modes may be expressed as [11]

$$\Delta\lambda = \frac{\lambda^2}{\Delta n L}, \quad (1)$$

where λ is the geometric mean of the two adjacent peak wavelengths and L is the interferometer cavity length, i.e., separation between the two tapers. As shown in Fig. 3(b), the fringe periodicity around $1570.16\ \text{nm}$ is $1.048\ \text{nm}$, giving an index difference of $\Delta n=0.102$. This value is much higher than those obtained from index-guiding photonic crystal fibers (IG-PCFs) [12] and conventional SMFs [13], which are typically of the order of 10^{-3} . The extremely high value of Δn would be beneficial for the construction of compact in-fiber modal interferometers, as it can significantly shorten the cavity length required to produce a reasonable number of fringes in a limited wavelength range.

We investigated the possible coupled modes theoretically and experimentally. The PBF was numerically studied by using a full-vector finite-element method and a model structure as described in [14]. Simulation results indicate that the fundamental mode is possibly coupled to a surface mode, and the index difference between these two modes is calculated to be 0.095 , which is close to the measured value of 0.102 . The mode intensity pattern was experimentally examined by using a tunable laser and

an IR camera. Figure 4 shows the near-field intensity pattern observed at the location of ~ 2 mm to the taper waist. It is clearly observed that the intensity of the coupled mode is distributed along the innermost silica wall. In addition, we found the interference fringes hardly changed when an optical gel with $n_D=1.46$ was applied around the tapered region or along the cavity length, which further confirmed that the coupled mode is a well-confined surface mode of the PBF. We may then conclude that the fringes in Fig. 3(b) are the results of interference between the fundamental core and the surface modes.

The in-fiber core–surface mode interferometer was explored for strain and temperature measurement. Figure 5 shows the wavelength variation in the interference peak centered on 1569.76 nm when longitudinal strain was applied to the interferometer. The peak wavelength linearly decreased with strain and the sensitivity was measured to be -0.64 pm/ $\mu\epsilon$, which is smaller than those of MZIs based on IG-PCFs [12]. The blueshift of the interference peak with increasing strain is opposite to those based on conventional SMFs [15]. The temperature response of the in-fiber interferometer was studied by placing it inside an oven with temperature adjustable from ambient to 100°C . The interference peak wavelength as a function of temperature is also shown in Fig. 5. Linear curve fitting indicates that the thermal coefficient of the peak wavelength shift is 495.6 pm/ $(^\circ\text{C m})$, which is much higher than that of IG-PCF [12].

In summary, we have fabricated and characterized nonadiabatic tapers in an air-core PBF. The taper allows the coupling between the core and the surface modes over a broad wavelength range. By cascading two such tapers along the same PBF, an in-fiber modal interferometer was constructed. The differential refractive index between the coupled modes was measured to be about 0.1, which is much higher than

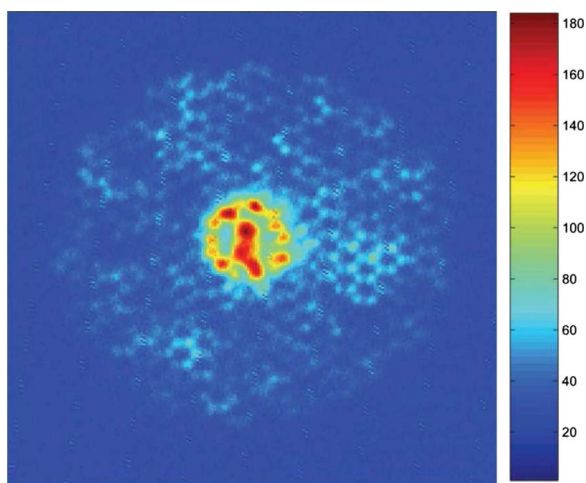


Fig. 4. (Color online) Near-field intensity pattern observed at a location of ~ 2 mm from the taper waist.

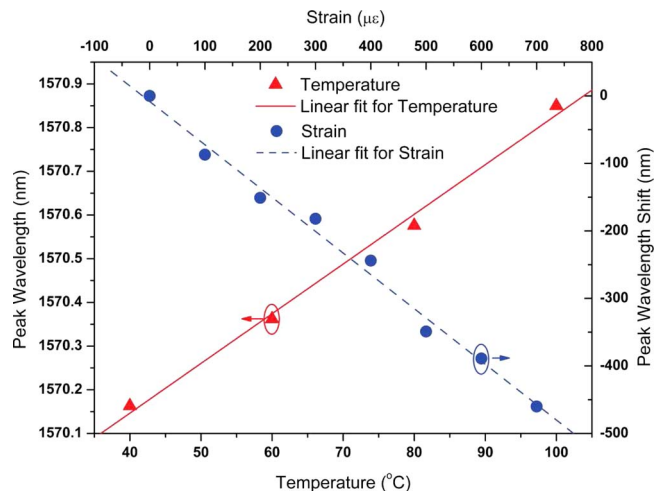


Fig. 5. (Color online) Temperature and strain response of the interference peak wavelength around 1570 nm.

those of conventional SMFs and IG-PCFs. The strain and the temperature sensitivities of the interferometer were measured to be -0.64 pm/ $\mu\epsilon$ and 495.6 pm/ $(^\circ\text{C m})$, respectively.

This work was supported by the Hong Kong Special Administrative Region Government through General Research Fund grant PolyU5182/07E.

References

1. R. F. Cregan, B. J. Mangan, J. C. Knight, T. A. Birks, P. St. J. Russell, P. J. Roberts, and D. C. Allan, *Science* **285**, 1537 (1999).
2. C. M. Smith, N. Venkataraman, M. T. Gallagher, D. Müller, J. A. West, N. F. Borrelli, D. C. Allan, and K. W. Koch, *Nature* **424**, 657 (2003).
3. M. Ohashi, K. Shiraki, and K. Tajima, *J. Lightwave Technol.* **10**, 539 (1992).
4. F. Benabid, J. C. Knight, G. Antonopoulos, and P. St. J. Russell, *Science* **298**, 399 (2002).
5. Y. L. Hoo, W. Jin, C. Shi, H. L. Ho, D. N. Wang, and S. C. Ruan, *Appl. Opt.* **42**, 3509 (2003).
6. Y. Wang, W. Jin, J. Ju, H. Xuan, H. L. Ho, L. Xiao, and D. N. Wang, *Opt. Express* **16**, 2784 (2008).
7. D. T. Cassidy, D. C. Johnson, and K. O. Hill, *Appl. Opt.* **24**, 945 (1985).
8. S. Lacroix, F. Gonthier, and J. Bures, *Opt. Lett.* **11**, 671 (1986).
9. J. D. Love, W. J. Stewart, W. M. Henry, R. J. Black, and S. Lacroix, *IEE Proc.-J: Optoelectron.* **138**, 343 (1991).
10. R. J. Black, S. Lacroix, F. Gonthier, and J. D. Love, *IEE Proc.-J: Optoelectron.* **138**, 355 (1991).
11. A. Ozcan, A. Tewary, M. J. F. Digonnet, and G. S. Kino, *Opt. Commun.* **271**, 391 (2007).
12. J. Ju, W. Jin, and H. L. Ho, *IEEE Photon. Technol. Lett.* **20**, 1899 (2008).
13. B. H. Lee and J. Nishii, *Appl. Opt.* **38**, 3450 (1999).
14. K. Saitoh, N. A. Mortensen, and M. Koshiba, *Opt. Express* **12**, 394 (2004).
15. Y.-G. Han, S. B. Lee, C.-S. Kim, J. U. Kang, U.-C. Paek, and Y. Chung, *Opt. Express* **11**, 476 (2005).